Original paper

The crystal structure of magnesian halotrichite, (Fe,Mg)Al$_2$(SO$_4$)$_4$·22H$_2$O: hydrogen bonding, geometrical parameters and structural complexity

Elena S. ZHITOVA[1]*, Rezeda M. SHEVELEVA[1,2], Andrey A. ZOLOTAREV[1,2], Sergey V. KRIVOVICHEV[2,3], Vladimir V. SHILOVSKIKH[1,2], Anton A. NUZHDAEV[1] and Maria A. NAZAROVA[1]

[1] Institute of Volcanology and Seismology, Russian Academy of Sciences, Bulvar Piypa 9, Petropavlovsk-Kamchatsky 683006, Russia; zhitova_es@mail.ru, zhitovaes@gmail.com;

[2] St. Petersburg State University, Universitetskaya Nab. 7/9, St. Petersburg 199034, Russia

[3] Nanomaterials Research Centre, Kola Science Centre, Russian Academy of Sciences, Fersman Street 14, Apatity 184209, Russia

*Corresponding author

The crystal structure of magnesian halotrichite has been refined for two samples collected as white efflorescences from the surface of geothermal fields associated with the Koshelevsky (sample **VK4-09**) and Centralny Semyachik (sample **SC2-20**) volcanoes (both Kamchatka peninsula, Russia). Halotrichite and its Mg-rich varieties are common products of the acid leaching of rocks, both volcanic and technogenic. The crystal structures of two halotrichite crystals were refined in the $P2_1/n$ space group (*vs.* $P2_1/c$ used previously) with the unit-cell parameters a = 6.1947(2)/ 6.1963(5) Å, b = 24.2966(8)/ 24.2821(14) Å, c = 21.0593(8)/ 21.063(2) Å, β = 96.512(4)/ 96.563(9) º, V = 3149.2(2)/ 3148.3(5) Å^3, Z = 4 to R_1 = 0.055 and 0.067 for 5673 and 3936 reflections with $I > 2σI$ reflections, respectively. The crystal structure consists of isolated Al(H$_2$O)$_6$ octahedra, SO$_4$ tetrahedra, H$_2$O molecules and [X(SO$_4$)(H$_2$O)$_5$]^0 clusters (X = Fe, Mg). The chemical analyses of both samples show their enrichment of Mg at the Fe^{2+} site. The analysis of geometrical parameters of the crystal structures of halotrichite and its Mg-analogue pickeringite suggests that the localization of O atoms carried out in this work is more accurate and the single-crystal X-ray diffraction data for the first time allowed localization of hydrogen atom positions. The refined number of H$_2$O molecules agrees with the ideal chemical formula. The crystal structure complexity of halotrichite is estimated as $I_{G,total}$ = 2305 bits/cell, which belongs to the family of very complex mineral structures. The contribution of hydrogen bonding system plays a significant role in the overall bonding scheme and the overall complexity of the crystal structure, increasing the Shannon information amount more than twice from $I_{G,total(noH)}$ = 988 bits/cell (no hydrogen atoms) to $I_{G,total}$ = 2305 bits/cell (all atoms including hydrogen). The comparative distribution of halotrichite relative to other Fe-Al hydrated sulfates from the standpoint of structural complexity is considered.

1. Introduction

Metal-sulfate salts are widespread in environments characterized by oxidizing conditions such as (i) the acid mine drainage (AMD), e.g., Iberian pyrite belt (SW Spain) (Espana et al. 2005), Kettara Mine (Morocco) (Hakkou et al. 2008), Baia Sprie mining area (Romania) (Buzatu et al. 2016), the Fornovolasco and Monte Arsiccio mines (Apuan Alps, Tuscany, Italy) (Biagioni et al. 2020; D'Orazio et al. 2021); (ii) volcanic fumaroles, e.g., Solfatara di Pozzuoli of Phlegrean Fields (Pozzuoli, Naples, Campania, Italy) (Russo et al. 2017), Donnoe fumarole field of Mutnovsky volcano, Kamchatka, Russia (Zhitova et al. 2022), Ebeco Volcano (Paramushir, Kuril Islands, Russia) (Shevko et al. 2018) and (iii) coal basins

including burning coal dumps, e.g., the Upper Silesian Coal Basin, South Poland (Kruszewski 2013; Matýsek et al. 2014), Bhanine Valley coals, South Lebanon (Kruszewski 2019) and Chelyabinsk Coal Basin, Russia (Chesnokov et al. 2008; Zolotarev et al. 2020a). According to their chemistry, metal-sulfate salts can be divided into sulfates of divalent cations, sulfates of trivalent cation, mixed divalent-trivalent salts and other sulfates, including those of monovalent cations (Jambor et al. 2000). The group of mixed divalent-trivalent salts includes halotrichite having the formula Fe^{2+}Al$_2$(SO$_4$)$_4$×22H$_2$O. The mineral belongs to the halotrichite group with the general formula XY_2(SO$_4$)$_4$×22H$_2$O, where X is a divalent cation and Y is a trivalent cation. The following cation pairs are known for the halotrichite-group minerals (with X : Y = 1 : 2): Mn^{2+}

Tab. 1. Crystal structure data for halotrichite and pickeringite from literature data and this work

Mineral	Pickeringite		Halotrichite				
Locality	Tucumcari, New Mexico, USA	Roccalumera, Messina, Italy	Alum Canyon, Patagonia Mountains, USA	Orphan mine, Grand Canyon, Coconino County, Arizona, USA	Recsk, Matra Mountains, Hungary	Verkne-Koshelevsky geothermal field of Koshelev volcano, Kamchatka, Russia	Severny Krater geothermal field of Bolshoy Semyachik volcano
Chemical formula	$(Mg_{0.88}Mn_{0.12})Al_2(SO_4)_4 \cdot 22H_2O$	$(Mg_{0.93}Mn_{0.07})Al_2(SO_4)_4 \cdot 22H_2O$	n. d.	$(Fe_{0.98}Ni_{0.02})Al_2(SO_4)_4 \cdot 22H_2O$	$(Fe_{0.99}Mg_{0.02}Mn_{0.01})Al_{1.98}(SO_4)_4 \cdot 22H_2O$	$(Fe_{0.7}Mg_{0.3})Al_2(SO_4)_4 \cdot 22H_2O$	$Al_2(SO_4)_4 \cdot 22H_2O$
Symmetry	Monoclinic	Monoclinic	Monoclinic	Monoclinic	Monoclinic	Monoclinic	Monoclinic
Space group	n. d.	$P2_1/c$	n. d.	Monoclinic	$P2_1/c$	$P2_1/c^*$	$P2_1/c^*$
Unit cell parameters							
a, Å	6.180	6.184	6.184	6.203	6.195	6.195	6.196
b, Å	24.268	24.271	24.257	24.32	24.262	24.297	24.282
c, Å	21.217	21.226	21.230	21.32	21.262	21.267	21.265
β, °	100.31	100.33	100.33	100.37	100.30	100.31	100.26
V, Å³	3130.9	3134.6	3133.1	3165.0	3144.4	3149.2	3148.3
Structure refined	No	Yes	No	No	Yes	Yes	Yes
Reference	https://rruff.info/R060108	Quartieri et al. (2000)	https://rruff.info/R060118	https://rruff.info/R070673	Lovas (1986)	This work	

* the space group is transformed to $P2_1/c$ from $P2_1/n$ in order to compare unit cell parameters; the unit-cell parameters are also transformed and rounded accordingly.

and Al (apjohnite), Fe^{2+} and Fe^{3+} (bilinite), Zn and Al (dietrichite), Fe^{2+} and Al (halotrichite), Mg and Al (pickeringite), Fe^{2+} and Cr (redingtonite), Co and Al (wupatkiite). Halotrichite is the most widespread and the oldest (since the 18th century) known member of the group, followed by its Mg-analogue pickeringite, $MgAl_2(SO_4)_4 \times 22H_2O$, due to the high abundance of specie-defining cations of these minerals in nature. This study shows that the samples under investigation are members of the halotrichite-pickeringite isomorphic series.

For both halotrichite and pickeringite the crystal structure solution and refinement were reported once from the powder X-ray diffraction data for the samples from Recsk (Matra Mountains, Hungary) (Lovas 1986) and Roccalumera (Messina, Italy) (Quartieri et al. 2000). The minerals are isotypic and crystallize in the monoclinic space group $P2_1/c$, the reported unit-cell parameters (Tab. 1) are within the following ranges, $a = 6.18–6.20$, $b = 24.26–24.32$, $c = 21.22–21.32$ Å, $\beta = 100.3–100.4°$. The crystal structure of both minerals consist of isolated $Al(H_2O)_6$ octahedra, SO_4 tetrahedra, H_2O molecules and neutral clusters with the composition $[Me(SO_4)(H_2O)_5]^0$ built by $Me^{2+}O(H_2O)_5$ (Me = Fe, Mg) octahedra sharing a common corner with SO_4 tetrahedra (Ballirano 2006). The isolated polyhedra and clusters are linked into a three-dimensional crystal structure by hydrogen bonds. However, hydrogen sites and, thus, hydrogen bonding schemes have never been reported neither for halotrichite, nor for pickeringite. To the best of our knowledge, single-crystal X-ray diffraction data for halotrichite and pickeringite have not previously been obtained due to the thinness and curvature of their acicular crystals. The present work aims to fill this gap.

The crystal-structure complexity can be considered one of the fundamental numerical characteristics of inorganic compounds that reflects their stability, chemical-physical properties and transformation paths. The approach of numerical evaluation of structural complexity was developed by Krivovichev (2012, 2013, 2015) and summarized by Krivovichev et al. (2022). The approach is based upon quantitative estimates of structural Shannon information per atom (I_G) and per unit cell ($I_{G,total}$). In this paper, we investigate the crystal structure complexity of halotrichite and rank it among the structures of minerals, along with the evaluation of the contribution of hydrogen atoms to the total crystal structure complexity and comparing the obtained values with other hydrated sulfates, whose crystal structures consist of isolated polyhedra or isolated heteropolyhedral clusters.
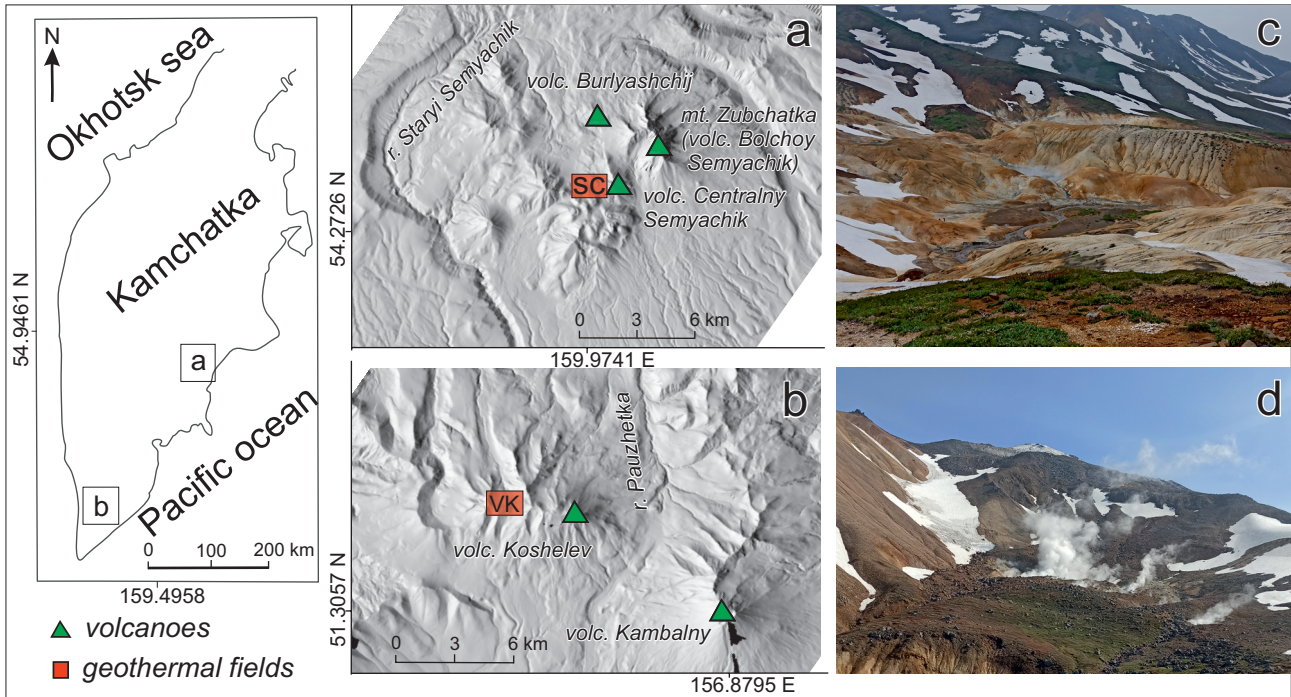
Fig. 1. Maps showing location of sampling sites. **a** – Verkhne-Koshelevsky (**VK**) and **b** –Severny Crater of Centralny Semyachik (**SC**) geothermal fields where the samples were collected. General views: **c** – Verkhne-Koshelevsky and **d** – Severny Crater of Centralny Semyachik geothermal fields.

2. Materials and methods

2.1. Samples collection

The samples of halotrichite have been collected from the surface of geothermal fields of southern Kamchatka (Russia) that are linked to the Koshelev and Bolshoy Semyachik volcanoes (Fig. 1). Among studied samples, in the **VK4-09** and **SC2-20** samples, white acicular halotrichite crystals of reasonable quality were found and selected for single-crystal X-ray diffraction studies. In general, it is worth noting that, according to X-ray powder diffraction data, halotrichite is widespread in the Kamchatka geothermal fields.

The sample **SC2-20** has been collected from the Severny (North) extinct Crater (SC) of Bolshoy Semyachik volcanic complex (Fig. 1a, c) on the edge of the heated thermal area representing patches of steaming ground. The efflorescence looked like a fluffy white crust up to 5 mm (Fig. 2a) in thickness formed mainly by acicular crystals of halotrichite. The surface temperature in the place of the collection was about 50 °C.

The sample **VK4-09** has been collected from the Verkne-Koshelevsky (VK) geothermal field associated to Koshelev volcano (Fig. 1b,d). The sample was selected from the aggregates that cover rock fragments at the mouth of a steam-gas vent (Fig. 2b). The estimated temperature at the site is about 60–70 °C.
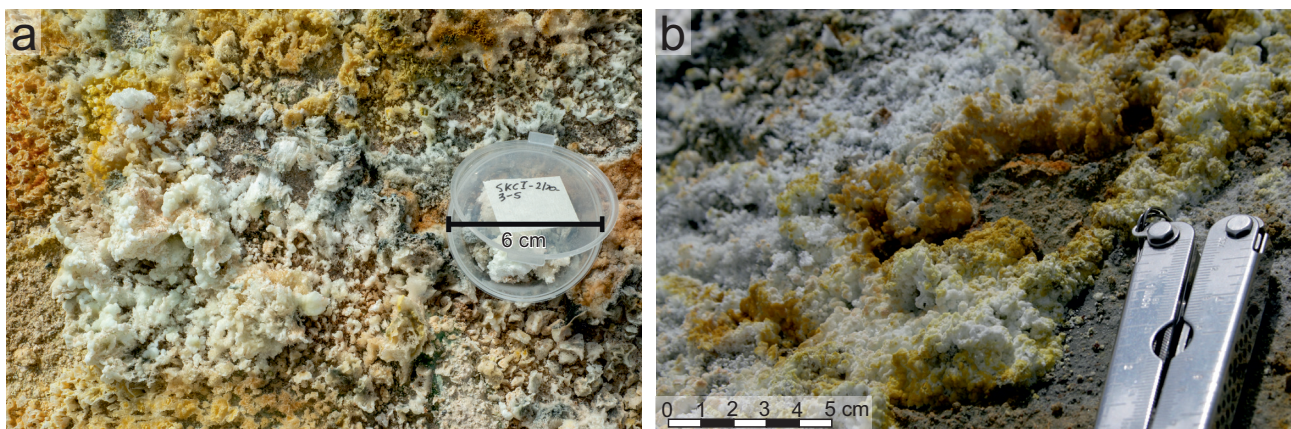
Fig. 2 Field photos. **a** – sample **SC2-20**, **b** – sample **VK4-09**.

Tab. 2. Chemical composition (in wt. %) of halotrichite

Sample	SC2-20 (another polished section)		VK4-09		Standard
Number of analyses	21		16		
Component	wt. %	*apfu*	wt. %	*apfu*	
MgO	2.09	0.46	1.20	0.26	MgO
FeO*	4.38	0.54	6.58	0.79	FeS_2
Al_2O_3	10.76	1.88	12.34	2.10	Al_2O_3
Fe_2O_3*	1.00	0.11	n. d.	n. d.	FeS_2
SO_3	36.15	4.01	34.71	3.76	FeS_2
SiO_2	n. d.	–	0.60	0.09	SiO_2
H_2O**	44.57	22.00	45.65	22.00	calc.
Total	**98.95**		**101.08**		

* divided based on the charge balance; ** calculated according to the stoichiometry of halotrichite (agrees with structure refinement reported therein).

apfu – atoms per formula unit; n. d. – not determined.

2.2. Methods

2.2.1. Chemical composition

The chemical composition of halotrichite was analyzed at the "Geomodel'" Resource Center of the Scientific Park of St. Petersburg State University on a Hitachi S-3400N scanning electron microscope, equipped with an Oxford X-Max 20 energy-dispersive spectrometer at an accelerating voltage of 20 kV, a probe current of 0.5 nA with various electron beam diameters of minimum 5 μm due to fast dehydration of halotrichite under the electron beam. The spectrometer was calibrated against the set of natural standards (MAC standards). The polished sections of both halotrichite samples were analyzed.

Tab. 3. Crystal data, data collection information and structure refinement parameters for halotrichite

	VK4-09	SC2-20
Crystal Data		
Space group	$P2_1/n$	$P2_1/n$
a (Å)	6.1947(2)	6.1963(5)
b (Å)	24.2966(8)	24.2821(14)
c (Å)	21.0593(8)	21.063(2)
β (°)	96.512(4)	96.563(9)
V (Å³)	3149.2(2)	3148.3(5)
Z	4	4
ρ_{calc} (g cm⁻³)	1.859	1.857
μ (MoK_α) (mm⁻¹)	0.809	0.795
Data collection and refinement		
Crystal size (mm)	0.2 × 0.07 × 0.05	0.15 × 0.05 × 0.05
$2\Theta_{max}$ (°)	64.74	60.00
Reflections collected	37196	29281
Unique reflections (R_{int})	9404 (0.0741)	8800 (0.139)
Unique reflections $I_o > 2\sigma I$	5673	3936
R_1 [for $I_o > 2\sigma I$]	0.0551	0.0671
wR_2 [for all data]	0.1124	0.1246
Goodness-of-fit on F^2	1.021	0.953
$\Delta\rho_{min/max}$ (e·Å⁻³)	–0.471/0.584	–0.450/0.467

The advantage of using the energy-dispersive mode instead of the wavelength-dispersive mode for studying hydrated metal sulfates and fumarolic minerals has been shown earlier (Kruszewski 2013; Balic-Žunic et al. 2016), since both short-time and low-probe current significantly contribute to preserving the studied material as noted in several works, including our previous study (Zhitova et al. 2022). Another advantage of energy-dispersive (ED) spectroscopy is the possibility of analyzing small-size grains of distinct minerals found in intimate association and *in situ* control of the sample condition during the spectrum acquisition.

2.2.2. Single-crystal X-ray diffraction

Single-crystal X-ray diffraction study of the halotrichite was performed using a four-circle diffractometer Rigaku Oxford Diffraction XtaLAB Synergy-S equipped with an HyPix-6000HE detector at the X-ray Diffraction Resource Center of St. Petersburg State University. The data were collected using monochromatic Mo$K\alpha$ radiation (λ = 0.71073 Å) at 50 kV and 1 mA. The structure data were integrated and corrected utilizing CrysAlisPro 1.171.41.104a (Rigaku Oxford Diffraction 2021), which was also used for an empirical absorption correction using spherical harmonics, implemented in SCALE3 ABSPACK scaling algorithm. The crystal was kept at 293(2) K during data collection. Using Olex2 (Dolomanov et al. 2009), the structure was solved with the SHELXS (Sheldrick 2008) structure solution program using direct methods and refined with the SHELXL (Sheldrick 2015) refinement package using least squares minimization. Crystal data, data collection information and structure refinement details for two halotrichite samples are given in Tab. 2. The hydrogen atoms were localized from the residual electron-density maps and refined using equivalent isotropic displacement parameter values restrained as 1.5 of (donor) oxygen atoms. Hydrogen O–H bonds have been constrained at 0.95(3) Å, and hydrogen bonds Ha···Hb have been constrained at 1.45–1.48 Å for both halotrichite samples.

2.2.3. Calculation of crystal structure complexity

Structural complexity of halotrichite and the other hydrated sulfates was estimated using the approach de-

veloped by Krivovichev (2012; 2013; 2015) and Krivovichev *et al.* (2022) that is based on the amount of Shannon information measured in bits per atom (I_G, bits/atom) and per unit cell ($I_{G,total}$, bits/cell), according to the following equations:

$$I_G = - \sum_{i=1}^{k} p_i \log_2 p_i, \qquad (1)$$

$$I_{G,total} = - v I_G =$$
$$= - v_i \sum_{i=1}^{k} p_i \log_2 p_i, \qquad (2)$$

where k is the number of independent crystallographic Wyckoff sites in the crystal structure, v is the total number of atoms in the reduced unit cell and p_i is the random choice probability for an atom from the i-th crystallographic site, p_i can be calculated by the equation (3):

$$p_i = m_i / v, \qquad (3)$$

where m_i is a multiplicity of a crystallographic position (i.e., the number of atoms of a specific Wyckoff site in the reduced unit cell).

All calculations of structural complexity in this research were implemented by means of the ToposPro software package (Blatov et al. 2014). We have estimated the structural complexity of halotrichite (our models) and other hydrated sulfates that contain isolated polyhedra and/ or finite clusters in their crystal structures. These minerals are reported from geothermal fields and geochemically similar environments. The following structural models were used (all included H positions): tschermigite (Abdeen et al. 1981), alum-(K) (Nyburg et al. 2000), alunogen (Menchetti and Sabelli 1974), ferricopiapite (Majzlan and Kiefer 2006), boussingaultite (Montgomery and Lingafelter

Tab. 4. Atom coordinates and equivalent isotropic displacement parameters (Ueq in Å^2) and site occupancies (s.o.f.) for halotrichite sample **VK4-09**

Site	x	y	z	U_{eq}	s.o.f.*
Fe	0.28688(8)	0.59562(2)	0.91907(2)	0.0196(2)	0.708(3)
Mg	0.28688(8)	0.59562(2)	0.91907(2)	0.0196(2)	0.292(3)
S1	0.57695(11)	0.46519(3)	0.61148(3)	0.0203(2)	1
S2	0.06032(11)	0.25697(3)	0.97343(3)	0.0210(2)	1
S3	0.05574(12)	0.47341(3)	0.89488(3)	0.0219(2)	1
S4	0.61518(12)	0.69379(3)	0.75664(3)	0.0216(2)	1
Al1	0.01571(13)	0.61261(3)	0.57565(4)	0.0179(2)	1
Al2	0.48743(13)	0.34344(3)	0.80178(4)	0.0181(2)	1
O1	0.1644(3)	0.66667(8)	0.62818(9)	0.0235(4)	1
H1A	0.2660(70)	0.6586(19)	0.6635(18)	0.118	1
H1B	0.2180(80)	0.6986(14)	0.6110(20)	0.118	1
O2	0.8748(3)	0.55766(8)	0.52312(10)	0.0259(4)	1
H2A	0.7650(60)	0.5650(19)	0.4913(19)	0.118	1
H2B	0.8430(80)	0.5227(12)	0.5370(20)	0.118	1
O3	0.3889(3)	0.26996(7)	0.78997(9)	0.0235(4)	1
H3A	0.4830(60)	0.2415(15)	0.7850(30)	0.118	1
H3B	0.2510(40)	0.2574(19)	0.7730(30)	0.118	1
O4	0.7675(3)	0.31651(8)	0.82995(10)	0.0253(4)	1
H4A	0.7910(80)	0.3018(19)	0.8700(12)	0.118	1
H4B	0.8550(80)	0.2983(19)	0.8062(18)	0.118	1
O5	0.7724(3)	0.61817(8)	0.62170(9)	0.0253(4)	1
H5A	0.6890(80)	0.5873(14)	0.6270(20)	0.118	1
H5B	0.7690(90)	0.6381(17)	0.6605(16)	0.118	1
O6	0.2570(3)	0.60846(8)	0.52893(10)	0.0250(4)	1
H6A	0.2580(90)	0.5838(18)	0.4944(18)	0.118	1
H6B	0.3420(80)	0.6376(16)	0.5190(30)	0.118	1
O7	0.1284(3)	0.55717(8)	0.63204(10)	0.0259(4)	1
H7A	0.0820(70)	0.5493(19)	0.6696(13)	0.118	1
H7B	0.2620(50)	0.5410(20)	0.6330(20)	0.118	1
O8	0.2041(3)	0.36826(8)	0.77563(10)	0.0272(5)	1
H8A	0.1280(80)	0.3933(18)	0.7979(18)	0.118	1
H8B	0.1640(80)	0.3770(20)	0.7333(8)	0.118	1
O9	0.5555(3)	0.34418(8)	0.71752(9)	0.0266(5)	1
H9A	0.5330(90)	0.3160(12)	0.6904(18)	0.118	1
H9B	0.5820(90)	0.3744(12)	0.6940(20)	0.118	1
O10	0.5300(3)	0.52273(8)	0.62708(10)	0.0291(5)	1
O11	0.9917(4)	0.61089(8)	0.95484(10)	0.0287(5)	1
H11A	0.9400(90)	0.6470(11)	0.9570(30)	0.118	1
H11B	0.9530(90)	0.5930(20)	0.9909(17)	0.118	1
O12	0.4414(3)	0.65401(8)	0.73501(10)	0.0323(5)	1
O13	0.4190(4)	0.34267(8)	0.88725(9)	0.0279(5)	1
H13A	0.3970(90)	0.3735(12)	0.9100(20)	0.118	1
H13B	0.3290(70)	0.3151(14)	0.9020(20)	0.118	1
O14	0.5849(3)	0.41546(8)	0.81424(10)	0.0266(5)	1
H14A	0.7330(30)	0.4212(19)	0.8250(30)	0.118	1
H14B	0.5270(70)	0.4491(12)	0.8010(20)	0.118	1
O15	0.8959(3)	0.66798(8)	0.52067(10)	0.0283(5)	1
H15A	0.7540(40)	0.6810(20)	0.5180(20)	0.118	1
H15B	0.9570(70)	0.6834(18)	0.4874(15)	0.118	1
O16	0.7958(3)	0.68844(8)	0.71664(10)	0.0343(5)	1
O17	0.7283(4)	0.46452(8)	0.56227(10)	0.0347(5)	1
O18	0.0147(3)	0.19927(8)	0.98832(10)	0.0291(5)	1
O19	0.1440(4)	0.28528(9)	0.95137(10)	0.0316(5)	1
O20	0.5757(3)	0.58478(9)	0.87531(11)	0.0301(5)	1

Tab. 4. Continued

Site	x	y	z	U_{eq}	s.o.f.[*]
H20A	0.6370(70)	0.6161(14)	0.8600(20)	0.118	1
H20B	0.6930(60)	0.5664(18)	0.8970(20)	0.118	1
O21	0.6816(3)	0.43762(8)	0.66895(10)	0.0312(5)	1
O22	0.5282(4)	0.75032(8)	0.74970(11)	0.0332(5)	1
O23	0.3772(4)	0.43597(9)	0.58840(10)	0.0379(6)	1
O24	0.8597(4)	0.49342(9)	0.92011(10)	0.0343(5)	1
O25	0.9945(3)	0.44410(9)	0.83381(10)	0.0331(5)	1
O26	0.1561(4)	0.63156(9)	0.82876(11)	0.0350(5)	1
H26A	0.0390(50)	0.6535(19)	0.8250(20)	0.118	1
H26B	0.2400(70)	0.6420(20)	0.7980(20)	0.118	1
O27	0.1952(4)	0.51950(8)	0.88070(11)	0.0371(6)	1
O28	0.1649(4)	0.28454(9)	0.03062(11)	0.0386(6)	1
O29	0.2060(4)	0.25802(8)	0.92307(11)	0.0395(6)	1
O30	0.3927(4)	0.67337(9)	0.95595(11)	0.0377(6)	1
H30A	0.5350(40)	0.6850(20)	0.9560(20)	0.118	1
H30B	0.3450(70)	0.6890(20)	0.9920(17)	0.118	1
O31	0.6975(4)	0.68252(9)	0.82292(10)	0.0415(6)	1
O32	0.1763(4)	0.43489(10)	0.93947(11)	0.0423(6)	1
O33	0.4070(4)	0.56093(13)	0.00756(14)	0.0570(8)	1
H33A	0.3220(60)	0.5410(20)	0.0330(20)	0.118	1
H33B	0.5490(40)	0.5510(20)	0.0200(20)	0.118	1
O34	0.0766(4)	0.39070(10)	0.65724(11)	0.0392(6)	1
H34A	0.0590(50)	0.4100(20)	0.6490(18)	0.118	1
H34B	0.1750(70)	0.4128(19)	0.6370(20)	0.118	1
O35	0.4428(5)	0.50971(10)	0.76575(12)	0.0448(6)	1
H35A	0.4640(70)	0.5375(14)	0.7960(15)	0.085	1
H35B	0.5370(60)	0.5197(17)	0.7354(16)	0.085	1
O36	0.4486(6)	0.26267(14)	0.64090(13)	0.0787(11)	1
H36A	0.5560(50)	0.2485(18)	0.6174(19)	0.118	1
H36B	0.3360(60)	0.2730(20)	0.6098(19)	0.118	1
O37	0.9979(5)	0.70582(11)	0.41117(13)	0.0569(7)	1
H37A	0.0740(80)	0.7322(14)	0.3900(20)	0.118	1
H37B	0.9780(90)	0.6764(13)	0.3807(15)	0.118	1
O38	0.9487(5)	0.53973(12)	0.73819(12)	0.0564(7)	1
H38A	0.9360(80)	0.5020(9)	0.7481(17)	0.118	1
H38B	0.0330(70)	0.5537(17)	0.7755(11)	0.118	1

[*] Chemical formula, based on structural analysis of sample **VK4-09** is $(Fe_{0.71}Mg_{0.29})Al_2(SO_4)_4 \cdot 22H_2O$

1964), melanterite (Baur 1964), and coquimbite (Demartin et al. 2010).

3. Results

3.1. Chemical composition

Twenty-one and sixteen EDS analyses were obtained for the determination of Mg, Fe, Al, S, and Si for the samples **SC2-20** and **VK4-09**, respectively. The contents of other elements with atomic numbers higher than that of carbon are below detection limits. The amount of H_2O was not analyzed because of the paucity of pure material (without intergrowth with other fine-grained sulfates). Instead, the H_2O content for each sample was calculated based on the

crystal-structure data. Analytical data are given in Tab. 2. In all analyses, Fe prevails over Mg, so all analyses are collected from halotrichite *sensu stricto* (not the mixture of halotrichite and pickeringite).

The empirical chemical formulas were calculated based on 7 cations $(Mg + Fe + Al + S + Si = 7)$. The chemical formula of the **SC2-20** sample is $(Fe^{2+}_{0.54}Mg_{0.46})_{\Sigma1.00}(Al_{1.88}Fe^{3+}_{0.11})_{\Sigma1.99}(SO_4)_{4.00} \cdot 22H_2O$. This sample is extremely rich in Mg, having the Mg : Fe ratio almost equal to 1 : 1, and the sample is very close to the intermediate halotrichite-pickeringite member. The chemical formula of the **VK4-09** sample is $(Fe^{2+}_{0.79}Mg_{0.26})_{\Sigma1.05}Al_{2.10}(\{S_{0.94}Si_{0.02}\}O_4)_{4.0} \cdot 22H_2O$ and can be considered as magnesian halotrichite. It should be noted that Si is very often found in sulfates in small amounts; most likely, it is an impurity. We note that these chemical formulas should be considered as general chemical characteristics of the samples. The chemical analyses were not carried out on the same needles from which the single crystal X-ray diffraction data were recorded since the single crystals were too minute for the sample preparation and reliable analytical study.

3.2. Structure refinement

The crystal structures of halotrichite samples **VK4-09** and **SC2-20** were solved and refined to $R_1 = 0.054$ and $R_1 = 0.067$ based on 5673 and 3936 unique observed reflections with $I > 2\sigma(I)$, respectively. The structures were refined in the space group $P2_1/n$ (#14) with the following unit-cell parameters given, along with other structure refinement parameters in Tab. 3. Atom coordinates, site occupancies and equivalent isotropic displacement parameters are provided in Tab. 4 and 5; anisotropic displacement parameters are presented in Tab. S1 and S2 (ESM1, 2). Selected bond lengths are given in Tab. 6. Crystallographic information files (cif) for the sam-

ples **SC2-20** and **VK4-09** are deposited at CCDC/FIZ Karlsruhe database under the CSD numbers 2210841 and 2210842, respectively. The parameters of the hydrogen bonding scheme are provided in Tab. 7. For the comparative purpose, we also carried out a refinement in the space group $P2_1/c$, the cif-files are presented in the form of supplementary materials and deposited at CCDC/FIZ Karlsruhe database under the CSD numbers 2212146 (**VK4-09**) and 2212145 (**SC2-20**). The study of halotrichite chemical composition has shown that Fe^{2+} is substituted by Mg (Tab. 2). Thus, we included Mg in the refinement as the second component to Fe in one (*Me*) site. The refinement of *Me* site occupancy has shown the following ratios: $Fe:Mg = 71:29$ and $68:32$ for **VK4-09** and **SC2-20**, respectively. The Fe:Mg ratios obtained by structure refinement agree well with the chemical composition data for sample **VK4-09** and somewhat differ for sample **SC2-20**, which is explained by the use of different crystals for these two research methods.

3.3. Crystal structure complexity

The results of the structural complexity calculations are represented in Tab. 8. The complexity calculated for the structural models, including H-atoms per atom and per unit cell, are marked as I_G and $I_{G,total}$, respectively. In contrast, complexity for models without H atoms per atom and per unit cell are marked as $I_{G(noH)}$ and $I_{G,total(noH)}$, respectively. From the data represented in Tab. 8, halotrichite is the most complex among the sulfate minerals, with crystal structures built from isolated

Tab. 5. Atom coordinates and equivalent isotropic displacement parameters (U in Å^2) and site occupancies (s.o.f.) for halotrichite sample **SC2-20**

Site	x	y	z	U_{eq}	s.o.f.*
Fe	0.28686(12)	0.59562(3)	0.91914(4)	0.0207(3)	0.675(4)
Mg	0.28686(12)	0.59562(3)	0.91914(4)	0.0207(3)	0.325(4)
S1	0.57701(18)	0.46509(4)	0.61143(6)	0.0208(3)	1
S2	0.06016(18)	0.25710(4)	0.97348(6)	0.0227(3)	1
S3	0.05601(18)	0.47334(4)	0.89509(6)	0.0237(3)	1
S4	0.61549(18)	0.69366(4)	0.75675(6)	0.0232(3)	1
Al1	0.0156(2)	0.61264(4)	0.57566(7)	0.0188(3)	1
Al2	0.4876(2)	0.34342(4)	0.80185(7)	0.0185(3)	1
O1	0.1637(5)	0.66664(10)	0.62801(16)	0.0230(7)	1
H1A	0.2720(70)	0.6600(20)	0.6627(19)	0.085	1
H1B	0.2140(80)	0.6978(15)	0.6080(20)	0.085	1
O2	0.8757(5)	0.55778(11)	0.52348(17)	0.0265(8)	1
H2A	0.7710(80)	5650(20)	0.4880(20)	0.085	1
H2B	0.8450(90)	0.5217(11)	0.5350(30)	0.085	1
O3	0.3891(5)	0.26992(10)	0.79007(16)	0.0237(7)	1
H3A	0.4820(60)	0.2432(17)	0.7780(30)	0.085	1
H3B	0.2510(40)	0.2590(20)	0.7720(30)	0.085	1
O4	0.7665(5)	0.31634(11)	0.82982(17)	0.0261(8)	1
H4A	0.7970(90)	0.3030(20)	0.8718(12)	0.085	1
H4B	0.8730(80)	0.3030(20)	0.8080(20)	0.085	1
O5	0.7732(5)	0.61817(11)	0.62162(16)	0.0253(8)	1
H5A	0.6860(80)	0.5879(15)	0.6300(30)	0.085	1
H5B	0.7740(90)	0.6384(18)	0.6598(17)	0.085	1
O6	0.2559(5)	0.60845(10)	0.5285.2(16)	0.0245(8)	1
H6A	0.2810(100)	0.5854(17)	0.4940(20)	0.085	1
H6B	0.3430(80)	0.6393(14)	0.5230(30)	0.085	1
O7	0.1278(5)	0.55738(11)	0.63199(16)	0.0266(8)	1
H7A	0.0900(80)	0.5520(20)	0.6737(14)	0.085	1
H7B	0.2640(50)	0.5400(20)	0.6330(30)	0.085	1
O8	0.2054(5)	0.36842(11)	0.77564(17)	0.0264(8)	1
H8A	0.1290(90)	0.3940(19)	0.7980(30)	0.085	1
H8B	0.1750(90)	0.3790(20)	0.7333(13)	0.085	1
O9	0.5558(5)	0.34414(11)	0.71755(16)	0.0273(8)	1
H9A	0.5290(90)	0.3182(15)	0.6841(19)	0.085	1
H9B	0.5850(100)	0.3767(12)	0.6970(20)	0.085	1
O10	0.5301(5)	0.52264(10)	0.62694(17)	0.0290(8)	1
O11	0.9923(5)	0.61075(11)	0.95471(17)	0.0289(8)	1
H11A	0.9520(90)	0.6477(10)	0.9570(30)	0.085	1
H11B	0.9400(100)	0.5940(20)	0.9900(20)	0.085	1
O12	0.4421(5)	0.65403(11)	0.73515(17)	0.0341(8)	1
O13	0.4198(5)	0.34257(11)	0.88713(17)	0.0288(8)	1
H13A	0.4210(100)	0.3715(18)	0.9160(20)	0.085	1
H13B	0.3230(80)	0.3179(19)	0.9040(30)	0.085	1
O14	0.5852(5)	0.41547(10)	0.81459(17)	0.0278(8)	1
H14A	0.7330(30)	0.4210(20)	0.8190(30)	0.085	1
H14B	0.5230(70)	0.4435(13)	0.7900(20)	0.085	1
O15	0.8961(5)	0.66819(11)	0.52081(17)	0.0287(8)	1
H15A	0.7510(40)	0.6800(20)	0.5170(30)	0.085	1
H15B	0.9470(100)	0.6810(20)	0.4839(16)	0.085	1
O16	0.7967(5)	0.68841(10)	0.71684(17)	0.0347(9)	1
O17	0.7288(5)	0.46452(10)	0.56221(16)	0.0342(9)	1
O18	0.0149(5)	0.19930(10)	0.98829(17)	0.0303(9)	1
O19	0.1442(5)	0.28520(11)	0.95130(16)	0.0312(8)	1
O20	0.5755(5)	0.58503(12)	0.87542(18)	0.0318(8)	1

Tab. 5. Continued

Site	x	y	z	U_{eq}	s.o.f.*
H20A	0.6420(80)	0.6171(14)	0.8630(30)	0.085	1
H20B	0.6910(60)	0.5658(18)	0.8980(30)	0.085	1
O21	0.6818(5)	0.43767(11)	0.66920(17)	0.0308(8)	1
O22	0.5284(5)	0.75024(11)	0.74971(17)	0.0325(9)	1
O23	0.3769(5)	0.43607(12)	0.58857(17)	0.0384(9)	1
O24	0.8596(5)	0.49352(11)	0.91994(17)	0.0369(9)	1
O25	0.9943(5)	0.44405(11)	0.83366(17)	0.0333(9)	1
O26	0.1566(6)	0.63164(12)	0.82906(18)	0.0349(9)	1
H26A	0.0290(50)	0.6520(20)	0.8200(30)	0.085	1
H26B	0.2370(80)	0.6420(20)	0.7960(20)	0.085	1
O27	0.1951(5)	0.51947(10)	0.88089(17)	0.0376(10)	1
O28	0.1650(5)	0.28457(11)	0.03103(18)	0.0389(9)	1
O29	0.2063(5)	0.25774(10)	0.92284(18)	0.0382(10)	1
O30	0.3931(5)	0.67335(12)	0.95586(19)	0.0374(9)	1
H30A	0.5340(40)	0.6890(20)	0.9600(30)	0.085	1
H30B	0.3280(100)	0.6850(20)	0.9920(20)	0.085	1
O31	0.6979(6)	0.68258(12)	0.82341(18)	0.0415(9)	1
O32	0.1767(6)	0.43510(12)	0.93941(19)	0.0443(10)	1
O33	0.4070(6)	0.56109(16)	0.0077(2)	0.0572(12)	1
H33A	0.3180(90)	0.5379(19)	0.0280(30)	0.085	1
H33B	0.5460(50)	0.5510(20)	0.0260(30)	0.085	1
O34	0.0766(6)	0.39069(12)	0.65753(19)	0.0395(9)	1
H34A	0.0570(40)	0.4099(19)	0.6490(20)	0.085	1
H34B	0.1700(70)	0.4131(18)	0.6370(30)	0.085	1
O35	0.4431(7)	0.50994(13)	0.7657(2)	0.0476(10)	1
H35A	0.4730(90)	0.5358(14)	0.7999(16)	0.085	1
H35B	0.5320(90)	0.5240(20)	0.7360(20)	0.085	1
O36	0.4507(9)	0.26327(18)	0.6410(2)	0.0830(16)	1
H36A	0.5430(50)	0.2410(17)	0.6210(20)	0.085	1
H36B	0.3260(60)	0.2670(20)	0.6120(20)	0.085	1
O37	0.9944(7)	0.70641(15)	0.4109(2)	0.0555(12)	1
H37A	0.1240(60)	0.7253(19)	0.4100(30)	0.085	1
H37B	0.9950(90)	0.6801(15)	0.3782(15)	0.085	1
O38	0.9489(7)	0.53981(17)	0.7378(2)	0.0569(11)	1
H38A	0.8800(90)	0.5056(13)	0.7390(30)	0.085	1
H38B	0.0570(80)	0.5410(20)	0.7730(20)	0.085	1

*Chemical formula, based on structural analysis of sample **SC2-20** is $(Fe_{0.68}Mg_{0.32})Al_2(SO_4)_4 \cdot 22H_2O$

polyhedra and clusters used for comparison. In general, the crystal structures of halotrichite and isotypic minerals (possibly all halotrichite group members) are highly complex.

Hydrogen positions significantly contribute to the complexity of hydrated sulfates with isolated complexes. The dependence of the structural complexity without considering of H-bonding system on the complexity of full structures, including H-positions, can be defined as a linear equation $I_{G(noH)} = 0.8646 \times I_G - 0.13$ ($R^2 = 0.99$) and $I_{G,total(noH)} = 0.4204 \times I_{G,total} + 33.123$ ($R^2 = 0.98$) (Fig. 4). Due to the fact that the structure of halotrichite is much more complex than that of hydrated sulfates (Tab. 8) with isolated units used for comparison, the contribution of hydrogen bonds to the crystal structure complexity of halotrichite per unit cell is very significant (Fig. 4b).

4. Discussion

4.1. Crystal structure and hydrogen bonding

The crystal structure of highly magnesian halotrichite studied in this work is isotypic to previously determined crystal structures of halotrichite, pickeringite, as shown in Fig. 3 and apjohnite reported previously (Menchetti and Sabelli 1976). However, the structure solutions and refinements carried out in this work are done in the space group $P2_1/n$ that is used for the first time, while previous refinements are done in the space group $P2_1/c$ (Lovas 1986; Quartieri et al. 2000). Space groups $P2_1/a$ and $P2_1/n$ are an example of an alternative space group setting $P2_1/c$. The crystal structure of halotrichite (and possibly isotypic halotrichite group minerals) can be solved and refined in either $P2_1/a$, $P2_1/c$, or $P2_1/n$ space groups with equal success, the choice of the space group in our case is caused by the smaller β angle (96.5 versus 100.3°). The transformation matrix from the space group $P2_1/c$ to $P2_1/n$ space group is -1 0 0 0 -1 0 1 0 1. The structural Tabs 3–7 provide data for structure refinement in the space group $P2_1/n$. The unit-cell parameters obtained for the refinement in the space group $P2_1/c$ are given in Tab. 1 (for comparison) and agree well with the previously determined unit-cell parameters.

As noted above, in our study, hydrogen atoms have been localized for halotrichite for the first time. Five vertices of Me = Fe/Mg octahedra and six vertices of each of the two independent Al octahedra are hydrated, producing 17 H_2O molecules per formula unit. Another 5 H_2O molecules are located in the space between polyhedra; acceptors of hydrogen bonds, in this case, are oxygen atoms of SO_4 tetrahedra, H_2O molecules, and Fe/Mg-centered octahedra. In general, the system of hydrogen bonds is very close to that of apjohnite (Menchetti and Sabelli 1976). The total number of H_2O molecules is 22 per formula unit, as in the ideal chemical formula. During the refinement process, we checked the occupancy

Tab. 6. Selected bond lengths (Å) in the crystal structure of halotrichite

	VK4-09	SC2-20		VK4-09	SC2-20
Me*–O11	2.088(2)	2.083(3)	S1–O10	1.472(2)	1.472(3)
Me–O20	2.120(2)	2.119(3)	S1–O17	1.474(2)	1.477(3)
Me–O26	2.165(2)	2.160(3)	S1–O21	1.468(2)	1.471(3)
Me–O27	2.072(2)	2.071(3)	S1–O23	1.461(2)	1.459(3)
Me–O30	2.118(2)	2.116(3)	<S1–O>	1.469	1.470
Me–O33	2.103(2)	2.103(4)			
<*Me*–O>	2.111	2.109	S2–O18	1.471(2)	1.471(3)
			S2–O19	1.469(2)	1.467(3)
Al1–O1	1.888(2)	1.883(3)	S2–O28	1.464(2)	1.468(3)
Al1–O2	1.884(2)	1.875(3)	S2–O29	1.469(2)	1.476(3)
Al1–O5	1.887(2)	1.882(3)	<S2–O>	1.468	1.471
Al1–O6	1.883(2)	1.885(3)			
Al1–O7	1.877(2)	1.872(3)	S3–O24	1.463(2)	1.463(3)
Al1–O15	1.873(2)	1.873(3)	S3–O25	1.481(2)	1.488(3)
<Al1–O>	1.882	1.878	S3–O27	1.466(2)	1.465(3)
			S3–O32	1.468(2)	1.461(3)
Al2–O3	1.894(2)	1.893(3)	<S3–O>	1.470	1.469
Al2–O4	1.886(2)	1.880(3)			
Al2–O8	1.878(2)	1.873(3)	S4–O12	1.479(2)	1.475(3)
Al2–O9	1.870(2)	1.872(3)	S4–O16	1.481(2)	1.483(3)
Al2–O13	1.895(2)	1.891(3)	S4–O22	1.477(2)	1.477(3)
Al2–O14	1.860(2)	1.860(3)	S4–O31	1.457(2)	1.463(4)
<Al2–O>	1.881	1.878	<S4–O>	1.473	1.475

* *Me* = Fe, Mg.

of hydroxylated oxygen atoms (i.e., donors of hydrogen atoms) that appeared to be very close to 100 %. The number of 22 H_2O molecules for the halotrichite unit cell seems crystal chemically fixed.

The hydrogen bonding network in halotrichite is complex. The one type of H_2O molecules is located in the interpolyhedral cavities (O34, O35, O36, O37 and O38) and are involved in two-center bonds with the range of the H···A distances of 1.81–2.54 Å and the D–H···A angles of 117–172° (D and A are oxygen atoms that act as donors and acceptors of hydrogen bonds, respectively). The H_2O molecules with donor oxygen atoms coordinating *Me* site (O11, O20, O26, O30 and O33) are characterized by shorter H···A distances in the range 1.81–2.19

Fig. 3. The crystal structure of halotrichite obtained in this work. Note: SO_4 tetrahedra are yellow; $Al(H_2O)_6$ octahedra are blue; $Me^{2+}\phi_6$ (*Me* = Fe, Mg and ϕ = H_2O, O) octahedra are brown; O atoms are red; H atoms are white, hydrogen bonding is outlined.
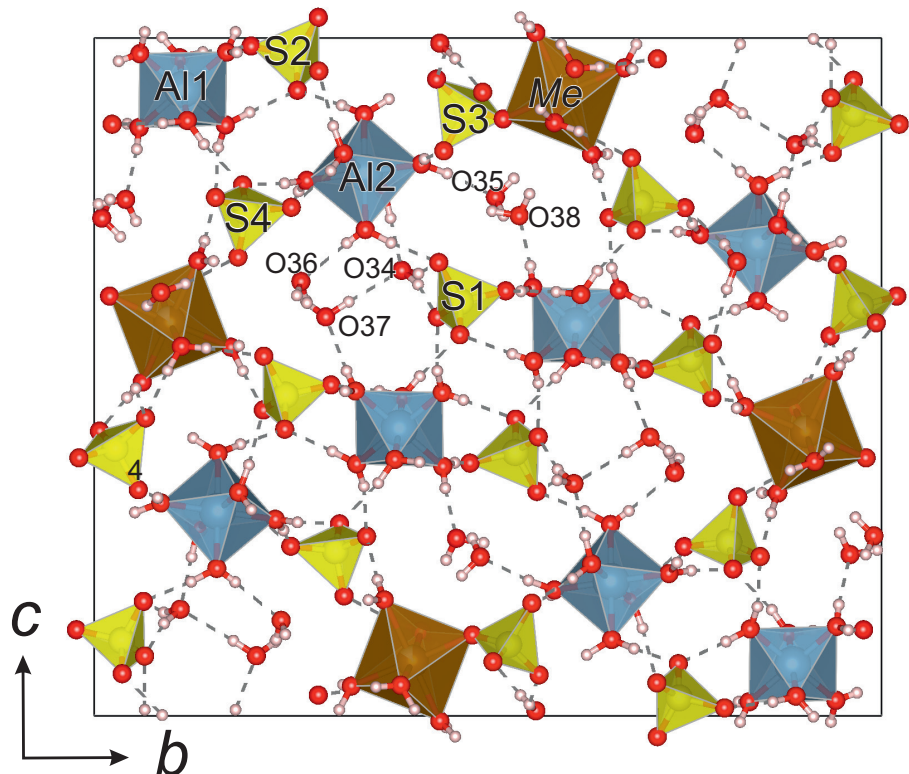
Å and D–H···A angles of 151–176°. The stronger two-center hydrogen bonds (Jeffrey 1997) are observed for H_2O molecules coordinating Al1 and Al2 sites with the range of the H···A distances of 1.64–1.91 Å and the D–H···A angles of 160–178 ° with one exception of longer (and weaker) bond O13–H13···O32 (H13···O32 = 2.26 Å; < O13–H13···O32 > = 135°). The geometries of the respective configurations are in agreement with those observed in hydrated salts (Jeffrey 1997). The calculation of bond valences (Tables S3, S4) shows that oxygen atoms coordinating metal cations (Al, Fe, Mg) receive ~ 0.33–0.50 valence units (*vu*) from metals and about 1.5 *vu* in the result of hydrogen bonding. At the same time, oxygen atoms of H_2O molecules located in the interpolyhedral cavities receive *vu* only as the result of hydrogen bonding.

4.2. Pickeringite-halotrichite solid solution: unit-cell parameters

Although it has long been suggested that complete isomorphic series between halotrichite and pickeringite exists (Ballirano 2006), the crystal structure refinements have been previously carried out for almost pure endmembers with the chemical formulas $(Fe_{0.99}Mg_{0.02}Mn_{0.01})$ $Al_{1.98}(SO_4)_4 \cdot 22H_2O$ and $(Mg_{0.93}Mn_{0.07})Al_2(SO_4)_4 \cdot 22H_2O$ for halotrichite and pickeringite, respectively (Tab. 1). Our structure refinements have been carried out for the Mg-rich halotrichite crystals with Fe^{2+}/Mg ~ 70/30. The chemical composition data (Tab. 2) show that the samples

Elena S. Zhitova, Rezeda M. Sheveleva, Andrey A. Zolotarev, Sergey V. Krivovichev, Vladimir V. Shilovskikh, Anton A. Nuzhdaev, Maria A. Nazarova
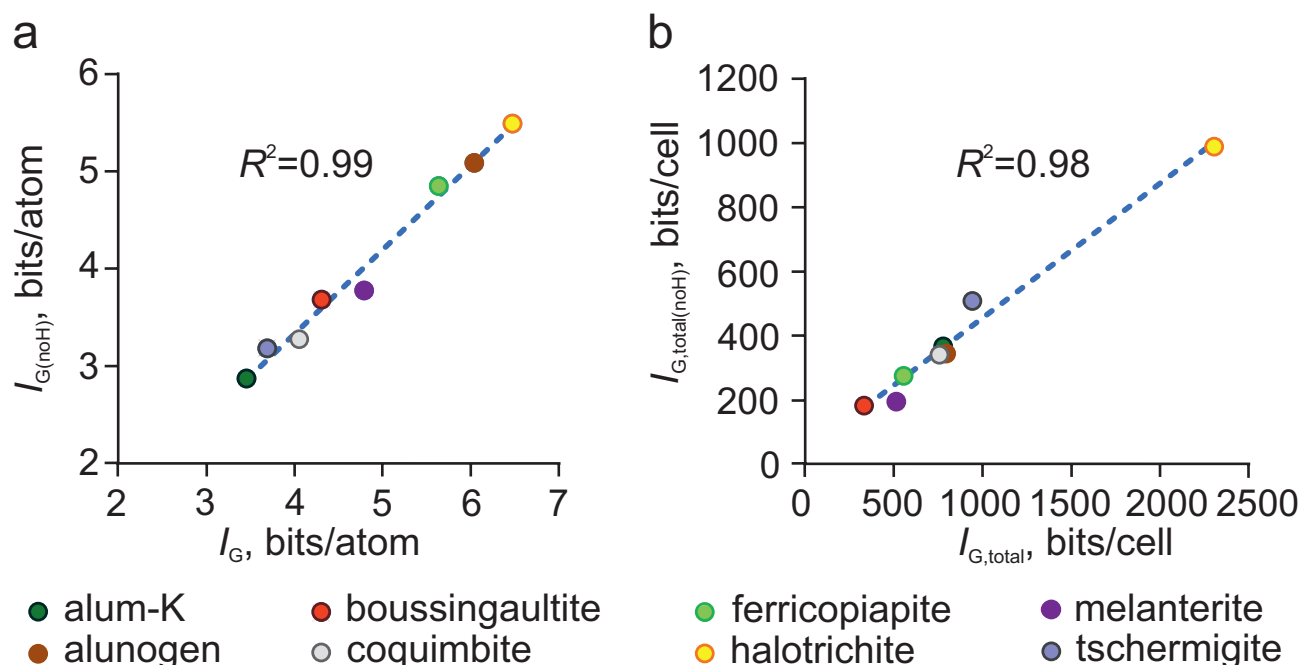
Fig. 4. The correlation between the crystal structure complexities, I_G (a) and $I_{G,total}$ (b) for the same structural models calculated for all atoms including (X-axis) and excluding (Y-axis) H atoms.

under study can even reach $Fe^{2+}/Mg \sim 50/50$, however, we did not come across crystals with such a low Fe^{2+}/Mg ratio when recording single-crystal X-ray diffraction data. The literature review shows that Mg-rich halotrichites are common. For instance, the variable Fe^{2+}/Mg ratio has been recently observed for halotrichite/pickeringite samples from Apuan Alps (Tuscany, Italy) by Mauro et al. (2019). The Mg-rich halotrichite with $Fe^{2+}/Mg \sim 63/37$ has been found in fumarolic deposits of White Island, New Zealand (Cody and Grammer 1979).

Since the cation radius of Fe^{2+} (0.92 Å) is larger than that of Mg (0.86 Å) (Shannon 1976), this should be expressed by the unit-cell parameters that can be used to identify minerals. The dependences of the unit-cell parameters *versus* the mean ionic radius of X^{2+} cation of synthetic analogues of halotrichite group were considered by Ballirano (2006) and have shown large departures from the linearity. The latter were explained by the different degree of filling of the *d*-electron shell. Here we provide characteristic ranges of the unit-cell parameters of halotrichite and pickeringite by summarizing structure data for these minerals (Tab. 1 for minerals and by Ballirano (2006) for their synthetic analogues). The comparison shows that the parameters for halotrichite from Orphan mine, Grand Canyon, Coconino County, Arizona, USA (Tab. 1), are too high, so they are not considered further as seemingly unrealistic. The clear difference between halotrichite and pickeringite is based on different unit-cell volumes. They range from 3142.3 to 3149.2 Å³ for halotrichite and its synthetic Mg-bearing analogue with Fe:Mg = 75:25, and from 3130.9 to 3134.6 Å³ for

pickeringite and its synthetic Fe-bearing analogue with Fe:Mg = 25:75. In this case, the unit-cell volume variation is < 0.25 %; such consistency of this value is surprising, taking into account the number of atomic positions in the unit cell. The difference between halotrichite and pickeringite is also clearly seen in the *a* unit-cell parameter in the ranges 6.191–6.196 Å and 6.180–6.188 Å for each of the minerals, respectively. The *b* unit-cell parameter varies in an incomprehensible way, being *b* = 24.297 Å and 24.282 Å for our samples with literally identical chemistry Fe/Mg ~ 70/30; for the synthetic sample with Fe/Mg = 75/25, *b* = 24.264 Å and, for the end-member halotrichite, *b* = 24.262 Å. Apparently, the *b* unit-cell parameter does not reflect the prevalence of the divalent cation. A significant difference between halotrichite and pickeringite is also detected by the *c* unit-cell parameter, which is in the range of 21.260–21.276 Å for halotrichite and in the range of 21.217–21.230 Å for pickeringite. The β angle for halotrichite and pickeringite is very similar and varies around the value of 100.29 ± 0.03° (in the $P2_1/c$ space group). Thus, the *a* and *c* unit-cell parameters and the corresponding volume can all be used to distinguish halotrichite from pickeringite, while the *b* unit-cell parameter and the β angle are not informative.

4.3. Pickeringite-halotrichite solid solution: bond distances and polyhedra distortion

The structure refinement of high-magnesium halotrichite makes it possible to compare crystal structures with different Fe^{2+}/Mg contents to reveal some of their crystal-

Tab. 7. Parameters of hydrogen bonding scheme for halotrichite samples **VK4-09** and **SC2-20**: **D** – donors, H – hydrogen atoms, **A** – acceptors, *d* – bond lengths (Å), < **D**-H···**A** angles (°)

	SC2–20				VK4–09			
D–H–A	*d*(D–H)	*d*(H···A)	<DHA	*d*(D···A)	*d*(D–H)	*d*(H···A)	<DHA	*d*(D···A)
O1–H1A···O12	0.949(14)	1.76(4)	170(5)	2.697(5)	0.938(19)	1.76(2)	170(5)	2.688(3)
O1–H1B···O29	0.935(19)	1.69(4)	174(5)	2.624(4)	0.939(19)	1.697(19)	175(5)	2.633(3)
O2–H2A···O23	0.942(19)	1.76(5)	163(5)	2.683(5)	0.916(19)	1.81(3)	157(5)	2.673(3)
O2–H2B···O17	0.933(19)	1.69(5)	164(6)	2.606(4)	0.931(19)	1.69(2)	168(5)	2.606(3)
O3–H3A···O16	0.925(19)	1.90(4)	161(6)	2.792(4)	0.919(19)	1.884(19)	172(5)	2.796(3)
O3–H3B···O22	0.932(19)	1.75(3)	166(5)	2.670(5)	0.938(19)	1.75(2)	165(4)	2.667(3)
O4–H4A···O19	0.938(19)	1.73(3)	174(5)	2.665(5)	0.912(19)	1.76(2)	169(5)	2.664(3)
O4–H4B···O22	0.911(19)	1.91(5)	150(5)	2.736(5)	0.896(19)	1.86(2)	165(5)	2.735(3)
O5–H5A···O10	0.940(19)	1.85(5)	166(6)	2.775(4)	0.923(19)	1.853(19)	173(4)	2.772(3)
O5–H5B···O16	0.941(19)	1.70(4)	165(5)	2.624(5)	0.953(19)	1.70(2)	163(4)	2.621(3)
O6–H6A···O17	0.941(19)	1.69(5)	165(6)	2.616(5)	0.943(19)	1.68(2)	175(5)	2.623(3)
O6–H6B···O18	0.936(19)	1.73(5)	175(5)	2.669(4)	0.92(2)	1.76(2)	170(5)	2.667(3)
O7–H7A···O38	0.943(19)	1.72(4)	164(5)	2.635(6)	0.893(16)	1.758(17)	170(4)	2.642(3)
O7–H7B···O10	0.938(19)	1.72(4)	166(5)	2.645(5)	0.918(19)	1.74(2)	167(5)	2.638(3)
O8–H8A···O25	0.93(2)	1.70(6)	175(6)	2.635(5)	0.928(19)	1.71(2)	175(5)	2.635(3)
O8–H8B···O34	0.928(19)	1.67(4)	169(6)	2.582(6)	0.925(13)	1.663(14)	176(5)	2.587(3)
O9–H9A···O36	0.944(18)	1.65(4)	164(5)	2.577(6)	0.892(17)	1.71(2)	171(5)	2.593(4)
O9–H9B···O21	0.931(19)	1.72(5)	169(5)	2.643(5)	0.915(19)	1.76(2)	163(5)	2.644(3)
O11–H11A···O28	0.933(19)	1.83(4)	170(6)	2.751(4)	0.938(19)	1.81(2)	175(5)	2.749(3)
O11–H11B···O32	0.94(2)	1.87(5)	176(6)	2.801(6)	0.93(2)	1.87(2)	168(5)	2.793(3)
O13–H13A···O32	0.93(2)	2.26(6)	135(5)	2.985(5)	0.911(19)	2.16(5)	149(5)	2.977(4)
O13–H13B···O29	0.94(2)	1.70(5)	160(5)	2.605(5)	0.944(19)	1.67(2)	169(5)	2.601(3)
O14–H14A···O25	0.919(19)	1.71(3)	168(5)	2.615(5)	0.928(19)	1.70(2)	168(5)	2.618(3)
O14–H14B···O35	0.910(18)	1.75(4)	160(4)	2.625(5)	0.921(19)	1.71(2)	170(5)	2.619(3)
O15–H15A···O18	0.94(2)	1.70(3)	178(5)	2.642(5)	0.927(19)	1.716(19)	175(5)	2.641(3)
O15–H15B···O37	0.927(19)	1.71(4)	170(6)	2.629(6)	0.914(18)	1.74(2)	162(4)	2.625(3)
O20–H20A···O31	0.933(19)	1.85(5)	163(5)	2.752(5)	0.923(19)	1.85(2)	168(4)	2.759(3)
O20–H20B···O24	0.939(19)	2.07(5)	151(5)	2.922(5)	0.927(19)	2.08(5)	150(4)	2.922(4)
O20–H20B···O11		2.37(5)	123(4)	2.977(5)		2.36(4)	124(4)	2.978(3)
O26–H26A···O31	0.935(19)	2.19(4)	161(5)	3.090(6)	0.895(19)	2.23(4)	161(4)	3.089(4)
O26–H26B···O12	0.938(19)	1.93(6)	169(5)	2.853(6)	0.919(19)	1.937(19)	171(5)	2.848(3)
O30–H30A···O28	0.942(15)	1.96(3)	175(5)	2.906(5)	0.929(19)	1.99(3)	171(4)	2.909(4)
O30–H30B···O19	0.943(14)	1.89(6)	166(5)	2.812(6)	0.931(19)	1.92(2)	158(4)	2.806(3)
O33–H33A···O24	0.93(2)	1.81(7)	166(6)	2.718(6)	0.923(19)	1.793(19)	176(5)	2.714(3)
O33–H33B···O32	0.93(2)	1.82(4)	154(5)	2.692(6)	0.926(19)	1.84(3)	152(5)	2.695(3)
O34–H34A···O21	0.951(18)	1.85(4)	155(4)	2.736(5)	0.960(19)	1.83(3)	155(3)	2.736(3)
O34–H34B···O23	0.937(19)	1.81(6)	162(5)	2.721(6)	0.95(2)	1.80(3)	163(5)	2.719(3)
O35–H35A···O20	0.959(19)	2.03(4)	172(5)	2.984(6)	0.928(18)	2.08(4)	164(4)	2.983(4)
O35–H35B···O10	0.945(19)	2.30(5)	136(4)	3.048(6)	0.945(18)	2.28(4)	138(3)	3.046(4)
O36–H36A···O28	0.924(18)	2.21(5)	148(4)	3.030(7)	0.940(18)	2.17(5)	147(4)	3.035(5)
O36–H36B···O37	0.928(19)	2.09(4)	151(6)	2.942(7)	0.936(19)	2.13(4)	152(3)	2.958(5)
O37–H37A···O28	0.928(19)	2.23(5)	140(6)	2.994(5)	0.944(19)	2.53(4)	110(3)	2.991(4)
O37–H37B···O34	0.940(18)	1.91(4)	152(4)	2.772(5)	0.959(18)	1.83(2)	164(3)	2.764(4)
O38–H38A···O21	0.935(19)	2.44(5)	141(5)	3.230(5)	0.947(18)	2.67(4)	119(3)	3.236(4)
O38–H38A···O25		2.53(6)	117(5)	3.071(6)		2.28(4)	140(3)	3.067(4)
O38–H38B···O27	0.94(2)	2.39(5)	152(5)	3.256(6)	0.955(18)	2.47(3)	138(4)	3.247(4)
O38–H38B···O26		2.54(5)	120(4)	3.124(6)		2.29(4)	145(4)	3.116(4)

lographic features. Tab. 9 contains information on mean bond lengths, polyhedral volumes, distortion indices and quadratic elongations of polyhedra in the crystal structures of halotrichite and pickeringite with different Fe^{2+}/Mg ratios and negligible impurities of Mn, Ni. The analysis of the data shows that the dominance of Fe or Mg is reflected in the Fe/Mg–O bond lengths (and, thus, polyhedral volumes) that are higher for halotrichite with Fe^{2+}–O = 2.107–2.109 Å (V_{FeO6} = 12.40–12.47 Å³) *versus* pickeringite where Mg–O = 2.010 Å (V_{MgO6} = 10.76 Å³).

Tab. 8. Crystal structure parameters and information complexities of hydrated salts with crystal structures based upon isolated polyhedra and finite clusters calculated including H positions (I_G, $I_{G,total}$) and excluding H positions ($I_{G(noH)}$, $I_{G,total(noH)}$)

Mineral	Halotrichite	Tschermigite	Alum-(K)	Alunogen	Ferricopiapite	Boussingaultite	Melanterite	Coquimbite**
Chemical formula	$FeAl_2(SO_4)_4 \cdot 22H_2O$	$(NH_4)Al(SO_4)_2 \cdot 12H_2O$	$KAl(SO_4)_2 \cdot 12H_2O$	$Al_2(SO_4)_3 \cdot 17H_2O$	$FeFe_4(SO_4)_6(OH)_2 \cdot 20H_2O$	$(NH_4)_2Mg(SO_4)_2 \cdot 6H_2O$	$Fe(SO_4) \cdot 7H_2O$	$AlFe_3(SO_4)_6 \cdot 18H_2O$
Symmetry	Monoclinic	Cubic	Cubic	Triclinic	Triclinic	Monoclinic	Monoclinic	Trigonal
Space group	$P2_1/n$	$Pa3$	$Pa3$	$P\bar{1}$	$P\bar{1}$	$P2_1/a$	$P2_1/c$	$P\bar{3}c$
Unit cell parameters								
a, Å	6.20	12.248	12.1350	7.425	7.3926	9.383	14.072	10.917
b, Å	24.28	12.248	12.1350	26.9750	18.3806	12.669	6.503	10.917
c, Å	21.06	12.248	12.1350	6.0608	7.3361	6.22	11.041	17.083
α, °	90	90	90	90.03	93.933	90	90	90
β, °	96.6	90	90	97.66	102.212	107.05	105.57	120
γ, °	90	90	90	91.94	98.9	90	90	90
V, Å^3	3148	1837.365	1786.979	1202.376	957.232	706.895	973.287	1763.189
Z	4	4	4	2	1	2	4	4
ρ (g/cm^3)	1.857	1.639	1.763	1.761	2.206	1.694	1.897	2.063
I_G, $I_{G,total}$	6.476, 2305	3.694, 946	3.485, 780	6.044, 798	5.639, 558	4.311, 336	4.792, 517	4.058, 763
$I_{G(noH)}$, $I_{G,total(noH)}$	5.492, 988	3.183, 509	2.874, 368	5.087, 346	4.850, 276	3.684, 184	3.777, 196	3.276, 341
Reference	This work, Lovas (1986), Quartieri et al. (2000)	Abdeen et al. (1981)	Nyburg et al. (2000)	Menchetti and Sabelli (1974)	Majzlan and Kiefer (2006)	Montgomery and Lingafelter (1964)	Baur (1964)***	Demartin et al. (2010)****

* Isotypic to aluminocopiapite with identical structure complexity; ** The structure complexity of aluminocoquimbite, $Al_2Fe_2(SO_4)_6(H_2O)12 \cdot 6H_2O$, has been estimated based on Demartin et al. (2010) data and completely matched with that of coquimbite: $I_G = 4.058$, $I_{G(noH)} = 3.276$ bits/atom; $I_{G,total} = 763$, $I_{G,total(noH)} = 341$ bits/cell. *** The crystal structure of melanterite obtained by Mauro et al. (2018) has the same structure complexity as the model of Baur (1964). **** The crystal structure of coquimbite obtained by Mauro et al. (2020) has the same structure complexity as the model of Demartin et al. (2010).

According to the data given in Tab. 9, the dependence of the decrease of the average <Al–O> bond length from Mg-dominant pickeringite through Mg-rich halotrichite to Fe-end-member of halotrichite is observed for both $Al1(H_2O)_6$ and $Al2(H_2O)_6$ polyhedra. The reason for such behavior is not entirely clear. Sulfate tetrahedra, in general, are expectedly consistent in terms of bond lengths and polyhedral volumes. There are several deviations for two tetrahedra in the structure of halotrichite obtained by Lovas (1986). We attribute this to the low accuracy in the localization of oxygen atoms from powder X-ray diffraction data (Lovas 1986) compared to the refinement based on single-crystal X-ray diffraction data (this study) since some of the S–O bonds are too long. The lower accuracy in the localization of oxygen atoms is also reflected by (i) orders of magnitude higher distortion indices for all polyhedra (Tab. 9) in the model of Lovas (1986) compared to other structural models and (ii) different angles of polyhedral tilting. The crystal-chemical inconsistency of the pickeringite model obtained by Quartieri et al. (2000) has been noted by Ballirano (2006), since the Mg–O bonds were found to be shorter than expected, causing a bond-valence overbonding of the metal (Mg) site. In our view, this discrepancy is associated with the less precise determination of the positions of oxygen atoms from the powder X-ray diffraction data. Thus, despite the fact that our structural model of halotrichite is close to those obtained previously (for halotrichite and pickeringite), we consider the structural models presented here as more accurate in terms of the localization of oxygen atoms and the determination of the H sites. This conclusion is corroborated by the bond-valence calculations that were performed using the parameters reported by Gagne and Hawthorne (2015). The bond-valence sums incident upon the metal sites for the samples **VK4-09** and **SC2-20**, respectively, are equal to (in *vu*): 2.1 for the Fe^{2+} site; 3.2 for Al1 and Al2 sites; 6.05 and 6.03 for the S1; 6.05 and 6.03 for the S2 sites; 6.04 and 6.05 for the S3 site; 5.98 and 5.97 for the S4 site.

4.4. Complexity and stability of halotrichite

The factors responsible for the high structural complexity of halotrichite and isotypic compounds are the high number of independent atomic sites (that reflects the diversity of

Tab. 9. Comparison of geometrical parameters of the crystal structures of halotrichite, pickeringite and magnesian halotrichite

Mineral	Pickeringite	Magnesian halotrichite		Halotrichite
Occupancy of *Me* site* (*Me* = Fe, Mg)	$Mg_{0.93}Mn_{0.07}$	$Fe_{0.71}Mg_{0.29}$	$Fe_{0.68}Mg_{0.32}$	$Fe_{0.99}Mg_{0.02}Mn_{0.01}$
Reference	Quartieri et al. (2000)	**VK4-09**, this work	**SC2-20**, this work	Lovas (1986)
$Al1(H_2O)_6$				
Average bond length (Å)	1.914	1.882	1.878	1.869
Polyhedral volume (Å³)	9.05	8.89	8.83	8.61
Distortion index (bond length)	0.004	0.003	0.003	0.029
Quadratic elongation	1.009	1.0003	1.0003	1.0081
$Al2(H_2O)_6$				
Average bond length (Å)	1.913	1.881	1.878	1.861
Polyhedral volume (Å³)	9.20	8.865	8.83	8.55
Distortion index (bond length)	0.005	0.006	0.005	0.016
Quadratic elongation	1.0099	1.0003	1.0003	1.0037
$Me\phi_6$ (*Me* = Fe, Mg and ϕ = H_2O, O)				
Average bond length (Å)	2.010	2.111	2.109	2.109
Polyhedral volume (Å³)	10.76	12.48	12.44	12.47
Distortion index (bond length)	0.007	0.011	0.011	0.023
Quadratic elongation	1.0039	1.0034	1.0034	1.0028
$SO_4(1)$				
Average bond length (Å)	1.478	1.469	1.470	1.55
Polyhedral volume (Å³)	1.65	1.63	1.63	1.81
Distortion index (bond length)	0.008	0.003	0.004	0.120
Quadratic elongation	1.0014	1.0002	1.0002	1.0519
$SO_4(2)$				
Average bond length (Å)	1.478	1.468	1.471	1.506
Polyhedral volume (Å³)	1.65	1.62	1.63	1.66
Distortion index (bond length)	0.013	0.002	0.002	0.054
Quadratic elongation	1.0021	1.0001	1.0001	1.0410
$SO_4(3)$				
Average bond length (Å)	1.474	1.470	1.469	1.561
Polyhedral volume (Å³)	1.64	1.63	1.63	1.79
Distortion index (bond length)	0.014	0.004	0.006	0.030
Quadratic elongation	1.0012	1.0007	1.0008	1.0610
$SO_4(4)$				
Average bond length (Å)	1.478	1.473	1.475	1.476
Polyhedral volume (Å³)	1.65	1.64	1.64	1.60
Distortion index (bond length)	0.007	0.006	0.004	0.036
Quadratic elongation	1.0012	1.0002	1.0002	1.0219

* Given occupancy of Mg and Fe in magnesian halotrichite is based on structural analysis of samples **VK4-09** and **SC2-20**

structural units, ranging from isolated octahedra and tetrahedra to the octahedral-tetrahedral dimers) and high hydration state (about 45 wt. % of H_2O in the halotrichite composition). A similar idea was expressed earlier for apjohnite (Menchetti and Sabelli 1976) when the authors noted some difficulties in the refinement procedure because of the unusually high number of atoms (89) in an asymmetric unit. In the original review by Krivovichev (2013) on ranking minerals' crystal structures according to their complexities, apjohnite and the Mn-analogue of halotrichite ($I_{G,total}$ = 2305 bits/cell) were among twenty the most structurally complex minerals. However, in the last nine years, seven new minerals with more complex crystal structures were discovered and characterized: ewingite (Olds et al. 2017a), morrisonite and vanarsite (Kampf et al. 2016), paddlewheelite (Olds et al. 2018), gauthierite (Olds et al. 2017b), rowleyite (Kampf et al. 2017), meerschautite (Biagioni et al. 2016); in addition, the very complex crystal structure of ilmajokite was solved (Zolotarev et al. 2020b). Moreover, the structural complexity parameters have been calculated for other very complex minerals with previously unknown H positions. As a consequence, the list of the twenty most complex minerals given in 2013 (Krivovichev 2013) was revised (Krivovichev et al. 2022), with only seven minerals remaining compared to the 2013 list. The list of twenty most complex minerals in 2022 starts with ewingite having $I_{G,total}$ = 23478 bits/cell and ends with rogermitchellite with $I_{G,total}$ = 3019 bits/cell.

Despite the very high structural complexity, the conditions resulting in the formation of halotrichite are quite simple and assume the presence of rock-forming minerals and an acidic sulfur-containing solution. Under suitable conditions, the mineral aggregates grow in a few hours or days. That is, the mineral is structurally complex and, on the one hand, is formed in a fairly geochemically simple way. On the other hand, its formation is secondary and assumes the existence of primary minerals that serve as a source of elements for the formation of secondary metal sulfate salts. The thermodynamic stability of halotrichite is restricted by its vast solubility in water. As a consequence, the mineral constantly dissolves in and grows again from water. It has been noted previously that more complex structures are more stable for other hydroxylated and/or hydrated sulfates of Fe (Majzlan et al. 2018). Other Fe–Al hydrated sulfates that can form under the acidic conditions of geothermal fields (among known Fe–Al natural hydrated sulfates) include aluminocopiapite, $Al_{2/3}Fe^{3+}_4$ $(SO_4)_6(OH)_2 \cdot 20H_2O$ and coquimbite-group minerals: aluminocoquimbite, $Al_2Fe^{3+}_2(SO_4)_6(H_2O)_{12} \cdot 6H_2O$ and coquimbite, $AlFe^{3+}_3(SO_4)_6(H_2O)_{12} \cdot 6H_2O$. All these minerals have considerably lower structure complexity (Tab. 9) and do not form widely in the studied geothermal fields, occurring very locally. This may indirectly confirm the idea expressed by Majzlan et al. (2018) for the higher stability of hydrated and/or hydroxylated Fe sulfates having higher crystal structure complexity. On the other hand, a direct comparison of the halotrichite-group minerals with copiapite- and coquimbite-group minerals is complicated due to the presence of both di- and trivalent metal cations.

5. Conclusions

Two samples of halotrichite originating from Kamchatka geothermal fields have been studied by single-crystal X-ray diffraction and energy-dispersive X-ray spectroscopy. Both samples are represented by a magnesian variety of halotrichite. The refined crystal structure model contains 89 symmetrically independent sites: hydrogen atoms are localized for the first time and oxygen atoms sites are believed to be localized more accurately compared to previous studies of halotrichite and pickeringite based on powder X-ray diffraction data. This resulted in more realistic *M*–O bond lengths, polyhedra distortion parameters and a sum of bond valences for cation sites. The structural complexity is very high due to the high number of independent sites and high hydration state of the mineral. The latter parameter increases structural complexity more than twice.

References

ABDEEN AM, WILL G, SCHAFER W, KIRFEL A, BARGOUTH MO, RECKER K, WEISS A (1981) X-ray and neutron diffraction study of alums: II. The crystal structure of methylammonium aluminium alum III. The crystal structure of ammonium aluminium alum. Z Kristallogr 157: 147–166

BALIC-ŽUNIC T, GARAVELLI A, JAKOBSSON SP, JONASSON K, KATERINOPOULOS A, KYRIAKOPOULOS K, ACQUAFREDDA P (2016) Fumarolic Minerals: An Overview of Active European Volcanoes. In: NEMETH K (ed) Updates in Volcanology, from Volcano Modelling to Volcano Geology. InTech, Rijeka, Croatia, pp 267–322

BALLIRANO P (2006) Crystal chemistry of the halotrichite group $XAl_2(SO_4)_4 \times 22H_2O$: the X = Fe-Mg-Mn-Zn compositional tetrahedron. Eur J Mineral 18: 463–469

BAUR WH (1964) On the crystal chemistry of salt hydrates. III. The determination of the crystal structure of $FeSO_4 \times 7H_2O$ (melanterite). Acta Crystallogr 17: 1167–1174

BIAGIONI C, MOËLO Y, ORLANDI P, STANLEY CJ (2016) Lead-antimony sulfosalts from Tuscany (Italy). XVII. Meerschautite, $(Ag,Cu)_{5.5}Pb_{42.4}(Sb,As)_{45.1}S_{112}O_{0.8}$, a new expanded derivative of owyheeite from the Pollone mine, Valdicastello Carducci: occurrence and crystal structure. Mineral Mag 80: 675–690

BIAGIONI C, MAURO D, PASERO M (2020) Sulfates from the pyrite ore deposits of the Apuan Alps (Tuscany, Italy): A review. Minerals 10(12): 1092.

BLATOV VA, SHEVCHENKO AP, PROSERPIO DM (2014) Applied topological analysis of crystal structures with the program package ToposPro. Cryst Growth Des 14(7): 3576–3586

BUZATU A, DILL HG, BUZGAR N, DAMIAN G, MAFTEI AE, APOPEI AI (2016) Efflorescent sulfates from Baia Sprie mining area (Romania)—acid mine drainage and climatological approach. Sci Total Environ 542: 629–641

CHESNOKOV BV, SHCHERBAKOVA EP, NISHANBAEV TP (2008) Minerals of burned dumps of Chelyabinsk coal basin. Miass Institute of Mineralogy, Miass, Russia, pp 1–140 (in Russ)

CODY AD, GRAMMER, TR (1979) Magnesian halotrichite from White Island. N Z J Geol Geophys 22(4): 495–498

D'Orazio M, Mauro D, Valerio M, Biagioni C (2021) Secondary Sulfates from the Monte Arsiccio Mine (Apuan Alps, Tuscany, Italy): Trace-element budget and role in the formation of acid mine drainage. Minerals 11(2): 206 DOI 10.3390/min11020206

Demartin F, Castellano C, Gramaccioli C M, Campostrini I (2010) Aluminum-for-iron substitution, hydrogen bonding, and a novel structure-type in coquimbite-like minerals. Canad Mineral 48: 323–333

Dolomanov OV, Bourhis LJ, Gildea RJ, Howard JAK, Puschmann H (2009) OLEX2: a complete structure solution, refinement and analysis program. J Appl Cryst 42: 339–341

Espana JS, Pamo EL, Santofimia E, Aduvire O, Reyes J, Barettino D (2005) Acid mine drainage in the Iberian Pyrite Belt (Odiel river watershed, Huelva, SW Spain): geochemistry, mineralogy and environmental implications. Appl Geochem 20(7): 1320–1356

Gagne OC, Hawthorne FC (2015) Comprehensive derivation of bond-valence parameters for ion pairs involving oxygen. Acta Crystallogr B71: 561–578

Hakkou R, Benzaazoua M, Bussière B (2008) Acid mine drainage at the abandoned Kettara Mine (Morocco): 1. Environmental characterization. Mine Water Environ, 27(3): 145–159

Jambor JL, Nordstrom DK, Alpers CN (2000) Metal-sulfate salts from sulfide mineral oxidation. Rev Mineral Geochem 40(1): 303–350

Jeffrey GA (1997) An introduction to hydrogen bonding. New York: Oxford university press, 12.

Kampf AR, Hughes JM, Nash BP, Marty J (2016) Vanarsite, packratite, morrisonite, and gatewayite: four new minerals containing the $[As^{3+}V^{4+,5+}_{12}As^{5+}_{6}O_{51}]$ heteropolyanion, a novel polyoxometalate cluster. Canad Mineral 54: 145–162

Kampf AR, Cooper MA, Nash BP, Cerling TE, Marty J, Hummer DR, Celestian AJ, Rose TP, Trebisky TJ (2017) Rowleyite, $[Na(NH_4,K)_9Cl_4][V^{5+,4+}_{2}(P,As)O_8]_6 \cdot n[H_2O,Na,NH_4,K,Cl]$, a new mineral with a microporous framework structure. Amer Min 102: 1037–1044

Krivovichev SV (2012) Topological complexity of crystal structures: Quantitative approach. Acta Crystallogr A68: 393–398

Krivovichev SV (2013) Structural complexity of minerals: Information storage and processing in the mineral world. Mineral Mag 77: 275–326

Krivovichev SV (2015) Structural complexity of minerals and mineral parageneses: Information and its evolution in the mineral world. In: Danisi R, Armbruster T (eds) Highlights in Mineralogical Crystallography. Walter de Gruyter GmbH, Berlin, Germany, pp 31–73

Krivovichev SV, Krivovichev VG, Hazen RM, Aksenov SM, Avdontceva MS, Banaru AM, Gorelova LA, Ismagilova RM, Kornyakov IV, Kuporev IV, Morrison SM, Panikorovskii TL, Starova GL (2022) Structural and Chemical Complexity of Minerals: an Update. Mineral Mag 86(2): 183–204

Kruszewski Ł (2013) Supergene sulphate minerals from the burning coal mining dumps in the Upper Silesian Coal Basin, South Poland. Int J Coal Geol 105: 91–109

Kruszewski Ł (2019) Secondary sulphate minerals from Bhanine Valley coals (South Lebanon): a crystallochemical and geochemical study. Geol Q 63(1): 65–87

Lovas GA (1986) Structural study of halotrichite from Recsk (Mátra Mts., N-Hungary). Acta Geol Hung 29: 389–398

Matýsek D, Jirásek J, Osovský M, Skupien P (2014) Minerals formed by the weathering of sulfides in mines of the Czech part of the Upper Silesian Basin. Mineral Mag 78(5): 1265–1286

Majzlan J, Kiefer B (2006) An X-ray and neutron-diffraction study of synthetic ferricopiapite, $Fe_{14/3}(SO_4)_6(OD,OH)_2(D_2O,H_2O)_{20}$, and ab-initio calculations on the structure of magnesiocopiapite $MgFe_4(SO_4)_6(OH)_2(H_2O)_{20}$. Canad Mineral 44: 1227–1237

Majzlan J, Dachs E, Benisek A, Plášil J, Sejkora J (2018) Thermodynamics, crystal chemistry and structural complexity of the $Fe(SO_4)(OH)(H_2O)_x$ phases: $Fe(SO_4)(OH)$, metahohmannite, butlerite, parabutlerite, amarantite, hohmannite, and fibroferrite. Eur J Mineral 30(2): 259–275

Mauro D, Biagioni C, Pasero M (2018) Crystal-chemistry of sulfates from Apuan Alps (Tuscany, Italy). I. Crystal structure and hydrogen bond system of melanterite, $Fe(H_2O)_6(SO_4) \cdot H_2O$. Period Mineral 87: 89–96

Mauro D, Biagioni C, Pasero M, Skogby H (2019) Crystal-chemistry of sulfates From the Apuan Alps (Tuscany, Italy). III. Mg-rich sulfate assemblages from the Fornovolasco mining complex. Atti della Società Toscana di Scienze Naturali, Memorie, Serie A 126: 33–44

Mauro D, Biagioni C, Pasero M, Skogby H, Zaccarini F (2020) Redefinition of coquimbite, $AlFe^{3+}_{3}(SO_4)_6(H_2O)_{12} \cdot 6H_2O$. Mineral Mag 84(2): 275–282

Menchetti S, Sabelli C (1974) Alunogen. Its structure and twinning. Tschermaks Mineral Petrog Mitt 21: 164–178

Menchetti S, Sabelli C (1976) The halotrichite group: the crystal structure of apjohnite. Mineral Mag 40: 599–608

Montgomery H, Lingafelter E C (1964) The crystal structure of Tutton's salts. II. Magnesium ammonium sulfate hexahydrate and nickel ammonium sulfate hexahydrate. Acta Crystallogr 17: 1478–1479

Nyburg SC, Steed J, Aleksovska S, Petrusevski VM (2000) Structure of the alums. I. On the sulfate group disorder in the alpha-alums. Acta Crystallogr B56: 204–209

Olds TA, Plášil J, Kampf AR, Simonetti A, Sadergaski LR, Chen Y-S, Burns PC (2017a) Ewingite: Earth's most complex mineral. Geology 45: 1007–1010

Olds TA, Plášil J, Kampf AR, Škoda R, Burns PC, Čejka J, Bourgoin V, Boulliard J-C (2017b) Gauthi-

erite, $KPb[(UO_2)_7O_5(OH)_7]\cdot 8H_2O$, a new uranyl-oxide hydroxy-hydrate mineral from Shinkolobwe with a novel uranyl-anion sheet-topology. Eur J Mineral 29: 129–141

Olds TA, Plášil J, Kampf AR, Dal Bo F, Burns PC (2018) Paddlewheelite, a new uranyl carbonate from the Jáchymov district, Bohemia, Czech Republic. Minerals 8: 511

Quartieri S, Triscari M, Viani A (2000) Crystal structure of the hydrated sulphate pickeringite $(MgAl_2(SO_4)_4\cdot 22H_2O)$ X-ray powder diffraction study. Eur J Mineral 12(6): 1131–1138

Rigaku Oxford Diffraction (2021) Rigaku CrysAlisPro Software System, Version 1.171.41.104a

Russo M, Campostrini I, Demartin F (2017) I minerali di origine fumarolica dei Campi Flegrei: Solfatara di Pozzuoli (Napoli) e dintorni. Micro 15: 122–192

Shannon RD (1976) Revised effective ionic radii and systematic studies of interatomic distances in halides and chalcogenides. Acta Crystallogr A 32(5): 751–767

Sheldrick GM (2008) A Short History of SHELX. Acta Crystallogr A64: 112–122

Sheldrick GM (2015) Crystal structure refinement with SHELXL. Acta Crystallogr C71: 3–8

Shevko EP, Bortnikova SB, Abrosimova NA, Kamenetsky VS, Bortnikova SP, Panin GL, Zelenski M (2018) Trace Elements and Minerals in Fumarolic Sulfur: The Case of Ebeko Volcano, Kuriles. Geofluids, 2018: 1–16

Zhitova ES, Khanin DA, Nuzhdaev AA, Nazarova MA, Ismagilova RM, Shilovskikh VV, Kupchinenko AN, Kuznetsov RA, Zhegunov PS (2022) Efflorescent Sulphates with M^+ and M^{2+} Cations from Fumarole and Active Geothermal Fields of Mutnovsky Volcano (Kamchatka, Russia). Minerals 12: 600

Zolotarev AA, Krivovichev SV, Avdontceva MS, Shilovskikh VV, Rassomakhin MA, Yapaskurt VO, Pekov IV (2020a) Crystal Chemistry of Alkali–Aluminum–Iron Sulfates from the Burnt Mine Dumps of the Chelyabinsk Coal Basin, South Urals, Russia. Crystals 10: 1062

Zolotarev AA, Krivovichev SV, Cámara F, Bindi L, Zhitova ES, Hawthorne F, Sokolova E (2020b) Extraordinary structural complexity of ilmajokite: A multilevel hierarchical framework structure of natural origin. IUCrJ 7: 121–128

The RRUFF™ Project. Accesed on October 3, 2022, at https://rruff.info/R060108

The RRUFF™ Project. Accesed on October 3, 2022, at https://rruff.info/R060118

The RRUFF™ Project. Accesed on October 3, 2022, at https://rruff.info/R070673